DEVELOPMENTAL BIOLOGY

Modification of maternally defined H3K4me3 regulates the inviability of interspecific *Xenopus* hybrids

Qi Long[1,3]†, Kai Yan[2,4,5,6]†, Chendong Wang[1], Yanling Wen[2], Furong Qi[2], Hui Wang[1], Peng Shi[2,4,5,6], Xingguo Liu[3], Wai-Yee Chan[1,4,7], Xuemei Lu[2,4,5,6]*, Hui Zhao[1,4,7]*

Increasing evidence suggests that interspecific hybridization is crucial to speciation. However, chromatin incompatibility during interspecific hybridization often renders this process. Genomic imbalances such as chromosomal DNA loss and rearrangements leading to infertility have been commonly noted in hybrids. The mechanism underlying reproductive isolation of interspecific hybridization remains elusive. Here, we identified that modification of maternally defined H3K4me3 in *Xenopus laevis* and *Xenopus tropicalis* hybrids determines the different fates of the two types of hybrids as te×ls with developmental arrest and viable le×ts. Transcriptomics highlighted that the P53 pathway was overactivated, and the Wnt signaling pathway was suppressed in te×ls hybrids. Moreover, the lack of maternal H3K4me3 in te×ls disturbed the balance of gene expression between the L and S subgenomes in this hybrid. Attenuation of p53 can postpone the arrested development of te×ls. Our study suggests an additional model of reproductive isolation based on modifications of maternally defined H3K4me3.

INTRODUCTION

Speciation is an evolutionary process via which populations evolve into new and distinct species, and reproductive isolation prevents interspecific hybridization and maintains the stability of species. Studying the mechanism underlying the regulation of reproductive isolation is critical for understanding speciation.

Reproductive isolation can be classified into two groups: prezygotic barrier and postzygotic barrier. The prezygotic barrier refers to the failure of zygote formation, whereas the postzygotic barrier occurs after zygote production and induces failed development. Notably, the molecular mechanism underlying the functions of the postzygotic reproductive barrier remains largely unknown (*1*, *2*). Genetic incompatibility has been implicated in the reproductive barriers (*3*) of nonviable hybrids of fishes (*4*) and *Drosophila* (*5*); this incompatibility can manifest as chromosome number alterations (*6*), chromatin inversion (*7*, *8*), heterochromatin interactions (*5*, *9*), defined genomic region rearrangement (*2*, *10*), centromere repositioning (*11*–*13*), chromatin DNA deletion (*14*), etc. Currently, genetic incompatibility in hybridization is not well understood because interspecific hybridization often causes inviability and sterility in hybrid embryos (*6*).

Xenopus tropicalis and *Xenopus laevis* are two classic animal models for studies on developmental biology and genetics (*15*), while *X. laevis* is an allotetraploid harboring two sets of chromosomes from two different subgenomes—designated as L and S—and the balance of the two subgenomes during evolution is well established (*16*–*18*). These species can hybridize, yielding two types of hybrids with different fates. Fertilization of *X. tropicalis* eggs with *X. laevis* sperms (te×ls) produces embryonic lethal hybrids; however, the crossing of *X. laevis* eggs with *X. tropicalis* sperms (le×ts) produces viable hybrids (*15*), which are an ideal model for studying the mechanism underlying reproductive isolation. A recent study suggested that paternal chromatin incompatibility during *Xenopus* hybridization led to embryonic lethality in the te×ls hybrid (*19*). Deletions of chromosomal DNA from chromosome 3L (ch3L) and 4L (ch4L) have been reported in te×ls, and paternal chromosome loss was suggested to induce failed development in te×ls embryos. In contrast, no chromosomal DNA deletions have been reported in viable le×ts embryos (*19*). However, the mechanism underlying the genetic differences between the two hybrids has not been fully elucidated.

Besides paternal factors, maternal differences may affect reproductive isolation between *X. laevis* and *X. tropicalis* because the main difference between the two hybrid embryos is initially brought about by the composition of oocytes (*20*). Maternal factors are essential in regulating embryonic patterning and chromatin remodeling (*21*, *22*). In the present study, we investigated the maternal factors that regulate reproductive isolation between *X. laevis* and *X. tropicalis* using two hybrids. The expression of genes located in the deleted regions of ch3L and ch4L could be largely compensated by homologous genes from other subgenomes in the te×ls hybrid. Our results suggest that maternally defined H3K4me3 determines the different fates of the *X. laevis* and *X. tropicalis* hybrid embryos and that activation of the P53 signal pathway in hybridization plays a critical role in establishing reproductive

[1]Key Laboratory for Regenerative Medicine, Ministry of Education, School of Biomedical Sciences, Faculty of Medicine, The Chinese University of Hong Kong; GMU-GIBH Joint School of Life Sciences, the Guangdong-Hong Kong-Macau Joint Laboratory for Cell Fate Regulation and Diseases, Guangzhou Medical University, Hong Kong SAR, China. [2]State Key Laboratory of Genetic Resources and Evolution/Yunnan Key Laboratory of Biodiversity Information, Kunming Institute of Zoology, The Chinese Academy of Sciences, Kunming 650223, China. [3]Guangzhou Institutes of Biomedicine and Health, The Chinese Academy of Sciences, Guangzhou 511436, China. [4]Kunming Institute of Zoology Chinese Academy of Sciences, The Chinese University of Hong Kong Joint Laboratory of Bioresources and Molecular Research of Common Diseases, Hong Kong SAR, China. [5]University of Chinese Academy of Sciences, Beijing 100049, China. [6]Center for Excellence in Animal Evolution and Genetics, The Chinese Academy of Sciences, Kunming 650223, China. [7]Hong Kong Branch of CAS Center for Excellence in Animal Evolution and Genetics, The Chinese University of Hong Kong, New Territories, Hong Kong SAR, China.
*Corresponding author. Email: zhaohui@cuhk.edu.hk (H.Z.); xuemeilu@mail.kiz.ac.cn (XM.L.)
†These authors contributed equally to this work.

isolation. Our study sheds light on the effects of maternally defined epigenetic modifications on embryonic development.

RESULTS

Inviability of the *Xenopus* hybrids

A recent study suggested that paternal chromatin incompatibility renders te×ls hybrids inviable on the basis of the finding that chromatin incompatibility was noted only on the paternal L chromosomes originating from *X. laevis* (*19*). We wanted to further delineate the underlying mechanism and thus performed an interspecific hybridization assay using the two *Xenopus* species. In line with previous reports (*15*, *19*), the hybrid le×ts embryos generated via the fertilization of an *X. laevis* egg with *X. tropicalis* sperm developed well, exhibiting normal morphogenesis (Fig. 1A and fig. S1A). However, the fertilization ratio of *X. tropicalis* eggs crossed with *X. laevis* sperm was apparently low, and the te×ls hybrids suddenly stopped developing at around stages 9 and 10, demonstrating mushroom-like morphology during gastrulation and onward (Fig. 1A). Germ layer formation occurs in both types of hybrids, as revealed by the expression of *sox17a*, *xbra*, and *sox2* and endoderm, mesoderm, and ectoderm marker genes (Fig. 1B). However, the lethal hybrid te×ls revealed much higher levels of *sox17a* compared with wild-type (WT) embryos (*X. laevis* and *X. tropicalis*) or the le×ts hybrids (Fig. 1B and fig. S1B). The increased expression of *sox17a* indicates overgrowth of the endoderm layer, which may interfere with the interactions between the endoderm and mesoderm cells.

Compensation of transcription after chromosomal DNA deletion in te×ls hybrids

In a previous report, the te×ls hybrid embryos lost large fragments of chromosomal DNA in ch3L and ch4L. This chromosomal fragment deletion was assumed to be the cause of embryonic lethality (*19*). We also performed whole-genome sequencing (WGS) assays for the two hybrid embryos. The hybrid sequences were aligned with either the *X. laevis* or *X. tropicalis* genomic DNA sequence. Similar chromosomal fragment deletions were observed in ch3L (21172000–144000000) and ch4L (48462000–144084000) of the te×ls hybrids, as reported previously (fig. S2A) (*19*). Four loci within the deletion region of ch3L were selected on the basis of the WGS results, and quantitative polymerase chain reaction (qPCR) was performed to quantify the reduction in the te×ls embryo. Compared with *X. laevis*, all the tested loci showed apparent signal reductions; however, they retained evident signals in the te×ls embryos (fig. S2B), suggesting that not all cells in te×ls hybrids harbor the chromosomal fragment deletions.

We also tested whether genomic DNA deletion also occurs in the le×ts hybrids because the two hybrids contain the same pronuclei initially. WGS analysis identified a large number of small fragmental deletions in the le×ts hybrids (fig. S2, C and D). We noted 12.49, 15.41, and 9.69% DNA losses in the L, S, and T subgenomes of the le×ts embryos, respectively. Moreover, the percentages of DNA loss were 20, 14.13, and 7.70% in the L, S, and T subgenomes of the te×ls hybrids, respectively (fig. S2E and table S1). Unlike the other chromosomes, ch1L exhibited only slight DNA loss in both hybrids, whereas, in ch3L and ch4L, chromosomal DNA deletions occurred only in the te×ls hybrid embryos (fig. S2E). We accordingly amplified the representative gene loci of the DNA deletions, as revealed by WGS, using PCR; no amplicons were detected in the le×ts hybrids, suggesting complete DNA loss at the sites assessed (fig. S2, F and G). After checking dozens of embryos, we concluded that loss of genomic DNA also occurred in the le×ts hybrids. These data indicate that chromatin incompatibility is a common feature of interspecific hybridization between *X. laevis* and *X. tropicalis* and that loss of genomic DNA did not occur only in the te×ls hybrid embryos, as was thought previously (*19*).

The effects of the chromosomal DNA deletion in ch3L and ch4L of te×ls on embryonic development were also evaluated using RNA sequencing (RNA-seq). Gene expression profiles of the hybrid, *X. laevis*, and *X. tropicalis* embryos were generated. *X. laevis* embryos at the same developmental stages were set as the control group to evaluate the transcription of genes located in the deletion region in the te×ls and le×ts hybrids. As predicted, the transcription of most genes among the 2130 genes in the deletion region of ch3L and ch4L was considerably reduced owing to the chromosomal fragment deletion in the te×ls hybrids (fig. S3, A and B).

Although the expression of most genes located in the deletion region of ch3L and ch4L decreased in the te×ls hybrids, their homologs in ch3S and ch4S as well as in the *X. tropicalis* subgenomes may have compensated for the reduced expression of genes from ch3L and ch4L. We calculated the cumulative gene expression individually by summing up all three corresponding homologs as a homolog gene expression unit (HGEU) in the te×ls hybrid and compared the cumulative gene expression between the te×ls hybrid and *X. laevis* embryos. Only a few HGEUs showed notable alterations in ch3L and ch4L in the te×ls hybrids as compared with those in *X. laevis* or *X. tropicalis* embryos at stage 8 or 10, respectively (Fig. 1, C and D). Next, we compared the transcriptomes of the four different species and found that the global transcription pattern of the te×ls hybrids was similar to that of *X. tropicalis*, whereas the le×ts hybrids were more similar to *X. laevis* (Fig. 1, C and E, fig. S4A, and table S6). Comparison between the te×ls hybrids and *X. tropicalis* showed that the number of differentially expressed genes (DEGs) had increased, especially at stage 10 (Fig. 1F, fig. S4B, and table S6). However, almost equal numbers of DEGs with up-regulation and down-regulation were found in the comparison between the le×ts hybrids and *X. laevis* (Fig. 1E and fig. S4B). The DEGs of *cdkn1a* and *gadd45b*, which are two important members of the P53 pathway, were up-regulated, whereas those of *tcf7l1*, *fzd4*, *wnt4*, *wnt7b*, and *sfrp1*, which are members of the Wnt signaling pathway, were repressed (Fig. 1F). The Wnt signaling pathway is important in regulating germ layer differentiation and cell movement (*23*). Among the aforementioned components of the Wnt signaling network, *wnt4* and *wnt7b* are noncanonical Wnt ligands and have been implicated in regulating cell movement in the gastrula (*24*, *25*). Both *fzd4* and *tcf7l1* are involved in canonical and noncanonical Wnt signaling pathways (*26*–*30*).

Our observations highlight a broader dysfunction of global transcription in the te×ls hybrids. Furthermore, a genetic compensation was induced for gene loss in ch3L and ch4L. Thus, lethality in the te×ls hybrid embryos may not be caused by the loss of a subset of metabolism-related genes located in chromosomal deletions in ch3L and ch4L only.

Defect of the te×ls hybrids in embryonic development

We observed a higher degree of alteration in gene expression between the te×ls hybrids and *X. tropicalis* embryos than between

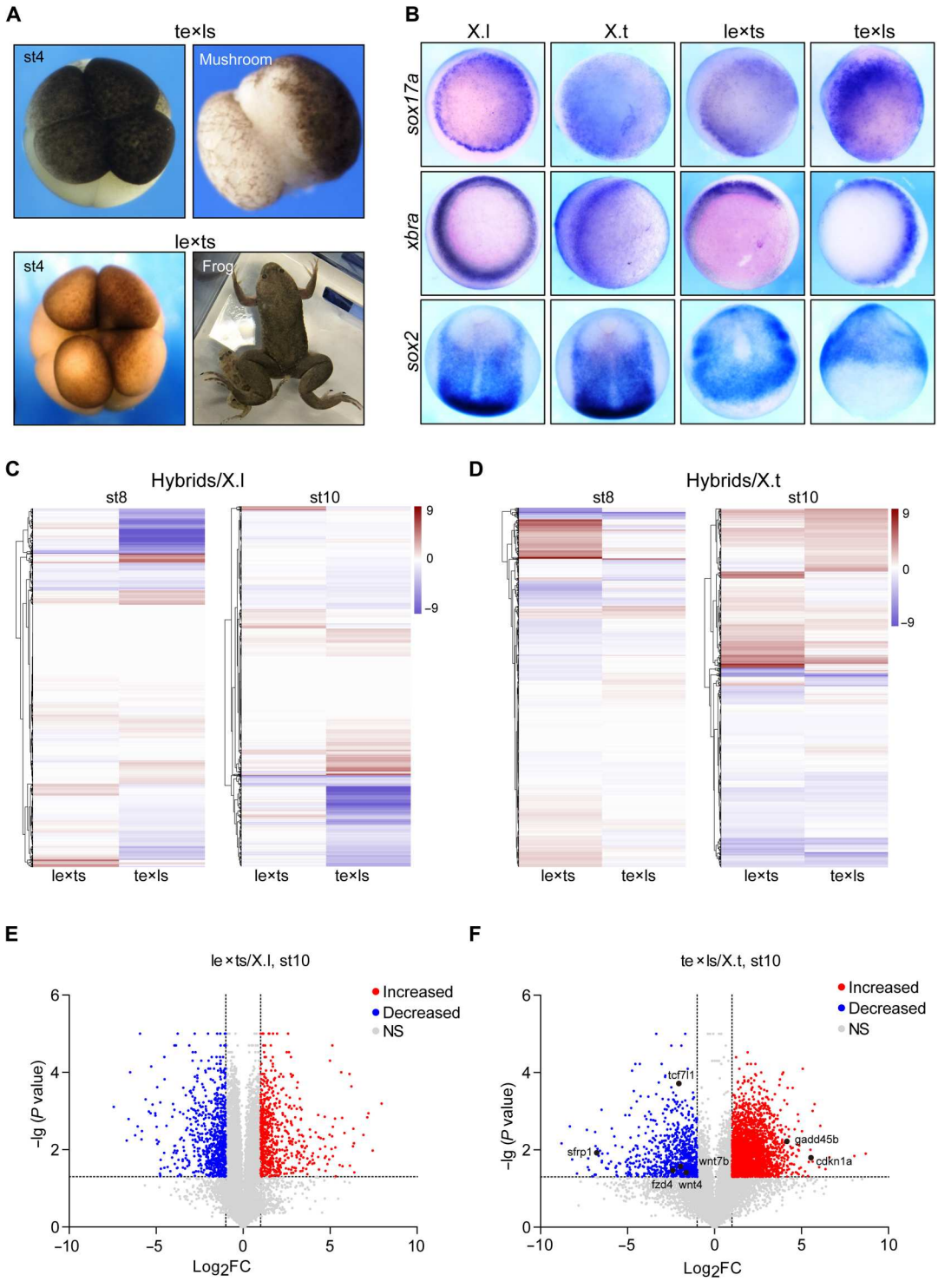

Fig. 1. Compensation of the chromosomal deletion in ch3L and ch4L by the homologs of *X. tropicalis* subgenomes. (**A**) Embryonic development of the te×ls hybrids (top) and le×ts hybrids (bottom). (**B**) Germ layer differentiation in wild-type (WT) embryos and hybrid embryos was detected by whole-mount in situ hybridization. *Sox17a* for endoderm, *xbra* for mesoderm, and *sox2* for ectoderm. le×ts and te×ls are the two types of hybrids. (**C** and **D**) Hierarchical clusters of HGEU expression in the comparison of the indicated hybrid versus *X. laevis* (C) or *X. tropicalis* (D) at the indicated stages. Individual HGEU values were generated by adding the expression values of the genes located in the lost region in ch3L and ch4L and the corresponding homolog gene from the subgenomes of *X. laevis* and *X. tropicalis*. The HGEU value was then normalized to the value of the corresponding HGEU in WT *X. laevis* (C) or *X. tropicalis* (D). (**E** and **F**) Volcano plots showing fold changes and *P* values of gene expression in the comparison between le×ts and the embryos of its maternal frog X.l at stage 10 (E) and the gene comparison between te×ls and its maternal frog X.t at stage 10 (F). The *x* axis represents the fold changes of HGEU, whereas the *y* axis represents the logarithm of the *P* value. The *P* value was generated by unpaired two-tailed *t* tests. NS, not significant; FC, fold change. X.l, *X. laevis*; X.t, *Xenopus tropicalis*.

le×ts hybrids and *X. laevis* (Fig. 1, E and F). Next, Kyoto Encyclopedia of Genes and Genomes (KEGG) pathway analysis was performed, which indicated the up-regulated pathways in the comparison between the te×ls hybrid and *X. tropicalis*. Among those pathways, DNA repair pathways—P53 signal pathway, homologous recombination (HR), nucleotide excision repair, base excision repair, and Fanconi anemia pathway (FA)—showed an apparent up-regulation in the te×ls hybrids compared with *X. tropicalis* (Fig. 2A). This result was in line with observations of large-scale DNA deletions in the te×ls hybrids (fig. S2, A and B). The P53, HR, and FA pathways were also highlighted upon performing gene set enrichment analysis (GSEA) (Fig. 2, B and C). Pathways related to lysine degradation, inositol phosphate metabolism, and pyruvate metabolism increased, whereas that related to folate biosynthesis

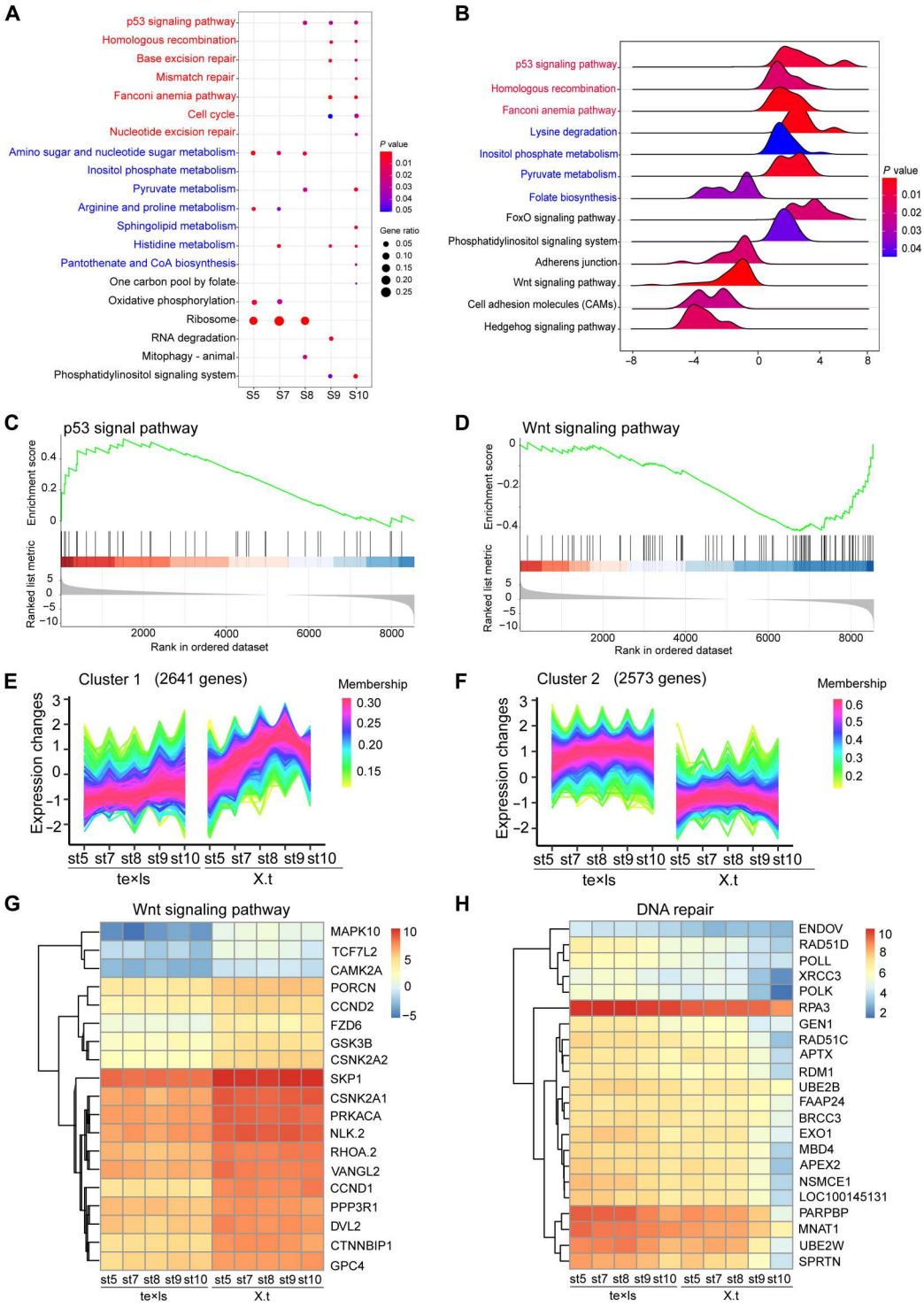

Fig. 2. Signaling pathways highlighted in the te×ls hybrids. (**A**) Dot plots showing the signaling pathways of the DEGs between the te×ls and *X. tropicalis* embryos from stages 5 to 10. The terms in red highlight denote the cell cycle and DNA damage repair. The terms in blue denote the metabolism pathway. The dot size represents the number of genes enriched by KEGG analysis, and the color of the dots represents the *P* value generated using the hyper geometric test. CoA, coenzyme A. (**B**) Ridgeline plot of GSEA between the te×ls hybrids and *X. tropicalis* embryos at stage 10. A negative value (<0) represents the pathways decreased in the te×ls hybrids, and a positive value (>0) represents the pathways increased in the te×ls hybrids. (**C** and **D**) The GSEA analysis of the P53 and Wnt signaling pathways between the te×ls hybrids and *X. tropicalis* embryos at stage 10. (**E** and **F**) Fuzzy c-means clustering identified 10 clusters with distinct temporal patterns of gene expression. The *x* axis represents the developmental stages in te×ls and X.t, whereas the *y* axis represents the values of normalized intensity considering the logarithm with base 2 at each stage. (**G** and **H**) Heatmap of DEGs involved in the Wnt pathway (G) and DNA damage repair (H) in the comparison of the te×ls hybrids and *X. tropicalis* from stages 5 to 10 are indicated. X.l, *X. laevis*; X.t, *X. tropicalis*.

decreased (*31*, *32*). The Wnt and HH signaling pathways were down-regulated (Fig. 2, B and D). In line with this finding, the expression of *nr3* and *siamois* (canonical Wnt target genes), and *vangl2* (a gene involved in noncanonical Wnt signaling), was reduced in te×ls compared to *X. tropicalis* embryos (fig. S5A). This finding is consistent with the loss of body axes and failure of morphogenetic movement in the developing te×ls hybrids, because the Wnt signaling pathway is essential for germ layer differentiation, axes formation, and embryonic patterning (*33*–*35*) (Fig. 1B). Together, our data suggest that rather than metabolic abnormalities only, a broad range of defects disturb developmental processes, resulting in the lethality of te×ls hybrid embryos.

To further understand failure in embryonic development, we conducted a cluster analysis for comparing the dynamic pattern

of transcripts between the lethal hybrids of te×ls and *X. tropicalis* in development; 10 clusters of gene expression with distinct dynamic patterns were generated (fig. S5, B to I, and table S5). Of the 10 clusters showing significant differences between the te×ls hybrids and *X. tropicalis* (Fig. 2, E and F), a subset of genes in cluster 1 was suppressed in the te×ls hybrids as compared with that in *X. tropicalis*; this cluster included genes belonging to both the canonical and noncanonical Wnt signaling pathways (Fig. 2, E and G, and fig. S5J). The dysregulation of canonical and noncanonical genes could count, at least in part, for the mushroom morphology of te×ls hybrid embryos, i.e., loss of dorsoventral and anteroposterior axis, and failure of morphogenetic movement during gastrulation. Another subset of genes belonging to cluster 2, which contains a large amount of DNA repair genes, exhibited hyperactivation (Fig. 2, F and H, and fig. S5K). Our findings are consistent with the activation of P53 signaling for sensing DNA damage in the te×ls hybrids.

Lack of epigenetic modifications in maternally defined H3K4me3 in the te×ls hybrids

X. laevis is an allotetraploid and contains two sets of two subgenomes—the L and S chromosomes. Each hybrid embryo contains three subgenomes, i.e., *X. laevis* L subgenome and S subgenome, and the *X. tropicalis* subgenomes (T subgenome). *X. laevis* has developed a unique mechanism to balance the two subgenomes during evolution (*16*–*18*). Although the mechanisms underlying compatibility between the two subgenomes remain elusive, a couple of studies have suggested that epigenetic factors play important roles in regulating incompatibility between the subgenomes (*16*, *18*). We, therefore, assessed epigenetic modifications in the hybrid and WT-type embryos using Western blotting. Unexpectedly, *X. laevis* embryos exhibited abundant histone modifications in H3K4me3 before gastrulation, whereas barely any H3K4me3 modifications were detected in *X. tropicalis* embryos (Fig. 3, A and B). H3K4me3 modification was suggested to be essential for balancing the L and S chromosomes in *X. laevis* (*17*, *18*). *X. tropicalis* embryos are diploid, containing two sets of chromosomes from one subgenome; its H3K4me3 becomes visible only at the onset of gastrulation (stage 10). Similar to *X. laevis* embryos, the le×ts embryos contained abundant H3K4me3 modifications (Fig. 3C). In contrast, the te×ls embryos lacked H3K4me3 modifications, showing a pattern similar to that of embryos from the maternal frog *X. tropicalis* (Fig. 3, D to F). This finding was confirmed by immunofluorescent staining of the embryos before gastrulation (Fig. 3, G and H). Moreover, the total level of H3 protein was maintained at the same level in embryos from stage 1 to 10, as revealed by Western blot (Fig. 3, A to D). Thus, H3K4me3 modifications in *Xenopus* embryos before gastrulation should be inherited mainly from the oocyte. The te×ls hybrids could not establish the H3K4me3 modification landscape even at stage 9, which is the important stage for preparing for gastrulation (Fig. 3G). Unlike H3K4me3, H3K9ac and H3K27ac showed a similar pattern in the four embryonic karyotypes. Their signals were barely detected before the mid-blastula stage (stage 8) but then increased and became evident (Fig. 3, A to D).

Imbalance among the three subgenomes in the te×ls hybrids

To study gene expression from the different subgenomes in the hybrids, we sorted all of the transcripts and mapped them to the corresponding L, S, and T subgenomes. In line with a previous study, in WT *X. laevis*, the L chromosomes prevailed over the S chromosomes (fig. S6, A and B) (*18*). The le×ts hybrids were similar to *X. laevis* embryos; their L chromosomes were shown to dominate the S chromosomes in transcription (fig. S6, C and D). However, the lethal hybrid te×ls embryos showed a different pattern of global gene expression. Maternal transcripts from the T subgenome were dominant before stage 9. Moreover, paternal subgenomes, including both L and S chromosomes, were activated since stage 9; however, the dominance of L to S was reversed. This group of genes—with a reverse pattern of L to S—were defined as unbalanced genes (fig. S6, E and F). At the same time, overall transcription from the T subgenome was maintained at the designated level (fig. S6E). As a result of evolution, the dominance of L over S chromosomes is apparently essential for the survival of *X. laevis*. A large number of elements in the S chromosome of *X. laevis* were gradually lost during evolution (*18*). The reversed activation of the S over the L subgenome in the te×ls hybrids, in turn, may activate a subset of silent genes, thus resulting in abnormal development of the te×ls hybrids. Together, our data suggest that the balance between the L and S chromosomes is disturbed in the te×ls hybrids, which may induce dysregulation in gene transcription of the subgenomes, consequently leading to failure of embryonic development in hybrids.

Contribution of H3K4me3 to development failures of the te×ls hybrids

H3K4me3 may play a critical role in balancing different subgenomes in the hybrids, as it does in *X. laevis*. To investigate the role of H3K4me3 in balancing the different subgenomes and its contribution to development failures in the te×ls hybrids, we analyzed the regulatory elements of H3K4me3 in both *X. laevis* and the te×ls hybrids. We obtained embryos of *X. laevis*, le×ts, and te×ls at stage 9 and performed chromatin immunoprecipitation sequencing (ChIP-seq) to delineate the landscape of H3K4me3 modifications in the three embryonic karyotypes. The ratio of H3K4me3 enrichment of the L chromosomes to that of the S chromosomes was reversed in the te×ls hybrids, as evident from the greater number of H3K4me3 peaks on S chromosomes; in contrast, the peaks were almost equally distributed in the L and S chromosomes in the *X. laevis* and le×ts hybrids (Fig. 4A). Notably, the high level of H3K4me3 modification corresponds to the gene expression in *X. laevis* (Fig. 4B and fig. S7A). The ratio of homolog gene expression of the L over the S subgenome also coincides with the H3K4me3 level, suggesting that H3K4me3 modifications regulate the balance between the L and S chromosomes. The imbalance in the H3K4me3 modifications between the L and S chromosomes may contribute to the reversal of gene transcription to favor the L over the S subgenome. In the te×ls embryos, the gene loci with H3K4me3 enrichment are highly overlapped with the genes lost in the dominance of L chromatin to S chromatin (Fig. 4, C and D). Among the 1238 gene loci with L/S imbalance, 1103 harbored H3K4me3 peaks (Fig. 4D). This observation suggests that H3K4me3 is involved in maintaining the balance of L and S chromatin. We further compared gene expression and H3K4me3 modifications between the te×ls and le×ts

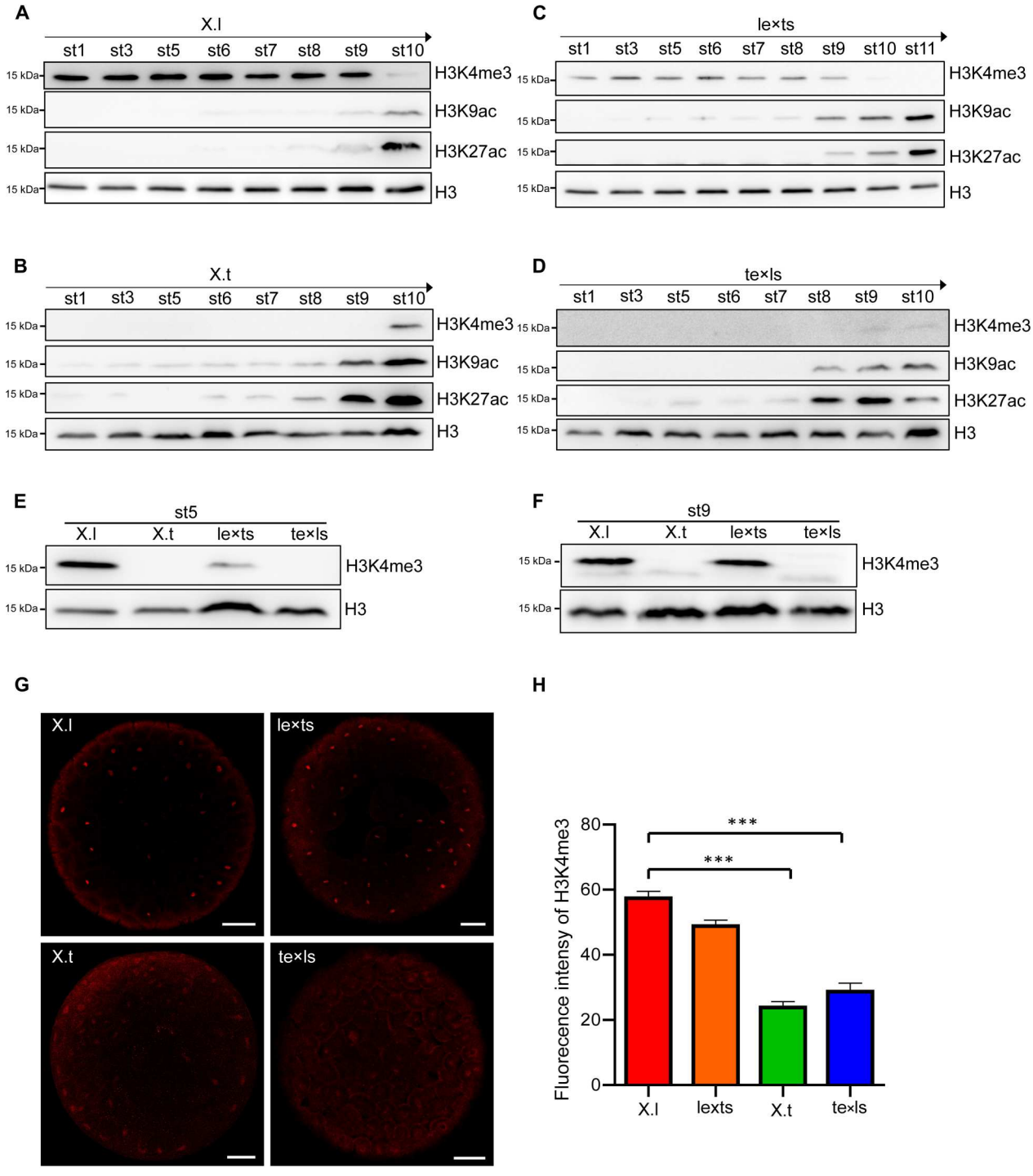

Fig. 3. The te×ls hybrids lack maternally defined H3K4me3 modifications. (**A** to **D**) Epigenetic modifications of H3K4me3, H3K9ac, and H3K27ac were detected using Western blotting of proteins extracted from the *X. laevis* (A), le×ts hybrid (B), *X. tropicalis* (C), and te×ls hybrid (D) embryos at the indicated stages. Histone H3 (H3) was used as the loading control. (**E** and **F**) H3K4me3 in the hybrids and WT embryos at stages 5 and 9. (**G**) Immunofluorescence staining shows H3K4me3 in the hybrids and WT *X. tropicalis* and *X. laevis* embryos. Eighteen embryos in each group from three independent experiments were detected. (**H**) Quantification of the abundance of the H3K4me3 embryos is shown in the left panel (G). At least 204 nuclei of 18 embryos in each group were counted. ***$P \leq 0.001$, using one-way analysis of variance (ANOVA) test. X.l, *X. laevis*; X.t, *X. tropicalis*.

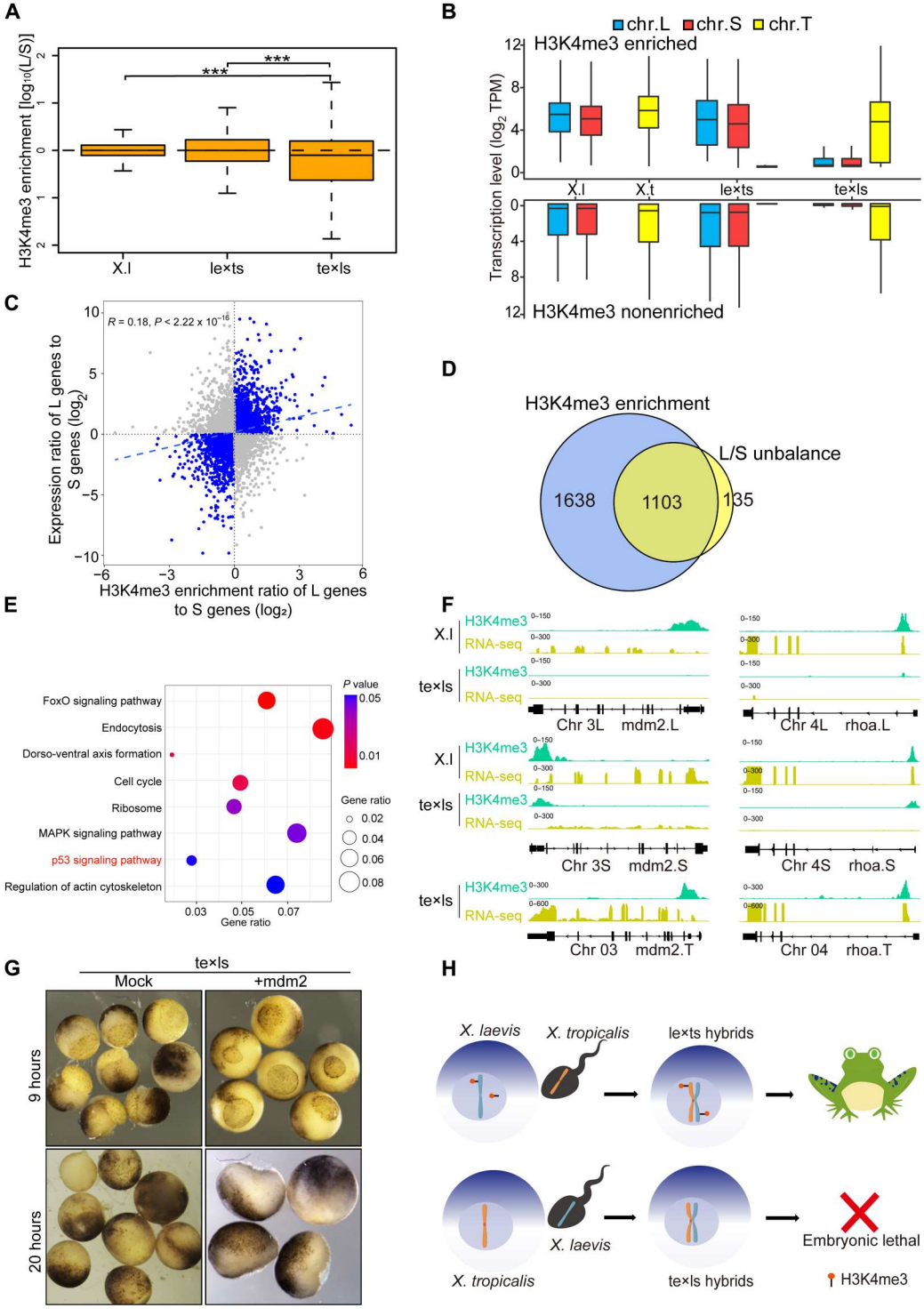

Fig. 4. Maternally defined H3K4me3 is involved in regulating differential transcription among the subgenomes in hybrids. (**A**) Comparison of the ratios of H3k4me3 enrichment in the L chromosome over the S chromosome in the *X. laevis*, le×ts, and te×ls embryos at stage 9. Wilcoxon rank sum test was used. ***$P \leq 0.001$. (**B**) Overall expression of genes with or without H3K4me3 enrichment in the L, S, and T chromosomes of *X. laevis*, *X. tropicalis*, le×ts, and te×ls embryos at stage 9. The gene expression level is represented as the logarithm transcript per million (TPM) to base 2. (**C**) The correlation between the gene expression ratio and H3K4me3 enrichment ratio of the L to S chromosomes in *X. laevis* (spearman $R = 0.18$, $P < 2.22 \times 10^{-16}$). (**D**) Venn diagram depicting the overlap of the H3K4me3-enriched genes and the genes showing unbalanced expression between the L and S chromosomes in the te×ls hybrids. (**E**) KEGG pathway analysis of the overlapping genes shown in (D). The dot size represents the number of genes enriched by KEGG analysis, and the color of the dots represents the *P* value generated using the hyper geometric test. MAPK, mitogen-activated protein kinase. (**F**) Representative genome views for H3K4me3 ChIP-seq track and transcripts in the *X. laevis*, le×ts, and te×ls hybrids. *mdm2.L*, *mdm2.S*, *mdm2.T*, *rhoa.L*, *rhoa.S*, and *rhoa.T*. (**G**) Overexpression of *mdm2* extended the development of the te×ls embryos to the neurula stage. (**H**) Schematic diagram illustrating that maternally defined H3K4me3 modifications regulate reproductive isolation in *X. laevis* and *X. tropicalis*, resulting in different fates of the two hybrids. X.l, *X. laevis* and X.t, *X. tropicalis*

hybrid embryos at stage 9; overall, the le×ts embryos contained a higher level of H3K4me3 modifications in all three subgenomes (fig. S7A). Among the 5317 genes with differential H3K4me3 levels, 4755 displayed significant changes in gene expression between the two karyotypes of embryos (fig. S7B). We also observed a differential H3K4me3 distribution among the compositions of the genome. In the le×ts hybrid, 59.66% of the H3K4me3 peaks were distributed in the exon and promoter regions, whereas this percentage was only 8.32% in the te×ls hybrid. In contrast, approximately 90% of the H3K4me3 peaks were found to lie in the intronic and intergenic regions of the te×ls hybrid, whereas this percentage was only 39.78% in the le×ts hybrid (fig. S7C). We also performed KEGG analysis to identify the overlapping genes (Fig. 4D). One of the important pathways highlighted by the KEGG analysis was the

P53 signal pathway (Fig. 4E), which was also identified in the transcriptomic analysis for the te×ls hybrid (Fig. 2C). Mdm2 is an E3 ubiquitin ligase responsible for the degradation of P53. In *X. laevis*, *mdm2.L* expression was higher than *mdm2.S* expression, and more intensive H3K4me3 peaks were found in *mdm2.L* than in *mdm2.S*. However, in the te×ls hybrids, the dominance of *mdm2.L* expression disappeared, and this was accompanied by the loss of H3K4me3; meanwhile, *mdm2.S* was up-regulated with an increase in H3K4me3 peaks (Fig. 4F). At the protein level, the total Mdm2 protein was reduced while P53 in was increased in te×ls compared to those in *X. tropicalis* embryos (fig. S8A). Moreover, *rhoa.L* and *rhoa.S*, which encode critical components in the noncanonical Wnt signaling pathway, showed a reversion similar to that shown by *mdm2.L* and *mdm2.S* (Fig. 4F), which was reflected in the observation of dysregulated Wnt signaling in the te×ls hybrids (Fig. 2, D and G).

Considerable DNA deletions were detected in both the te×ls and le×ts hybrids. P53 signaling is crucial in sensing DNA damage and facilitating DNA repair by activating cell cycle arrest (*36*). Using RNA-seq, we identified that P53 signaling was activated in the te×ls hybrid, and this was also highlighted by the KEGG analysis performed for genes with H3K4me3 enrichment and L to S subgenome reversion. We, therefore, tested whether the attenuation of P53 signaling could reverse arrested development in the te×ls hybrid. The *mdm2* mRNA was injected into the te×ls embryos at the one-cell stage. While the uninjected te×ls hybrid embryos stopped developing at the gastrula stage (9 hours after fertilization), more than two-thirds of the te×ls hybrid embryos after injection completed gastrulation successfully (105 of 123 embryos). However, the morphology of these embryos changed to abnormal at the neurula stage (approximately 20 hours after fertilization) (Fig. 4G). The *mdm2*-injected te×ls hybrid embryos could not complete the neural tube closure (fig. S8B). We examined the expression of *chordin*, *pax6*, *snail2*, and *sox2*, which can indicate the anteroposterior patterning at neurula stages, in either *mdm2*-injected te×ls hybrid or *X. tropicalis* embryos. The expression of *chordin*, *pax6*, and *snail2* is much reduced, while *sox2* signals remain diffused, compared to those in *X. tropicalis* embryos (fig. S8C). Thus, attenuation of P53 signaling partially rescued the arrested development of the te×ls hybrids. Because the inhibition of Kdm5 (including Kdm5a/b/c), the histone demethylase for H3K4me1/2/3, could improve H3K4me3 level in embryos (*37*), we treated te×ls hybrid embryos with the pan-Kdm5 inhibitor KDM5-C70 and found that the treatment could partially rescue the development arrest of the te×ls hybrids, and extend their development period at least to stage 11 (fig. S8D). Moreover, elevations of H3K4me3 and Mdm2 were observed in KDM5-C70–treated te×ls embryos (fig. S8E). These findings support that H3K4me3 regulates the inviability of the te×ls hybrids further.

DISCUSSION

Interspecific hybridization plays an important role in speciation. It is essential to understand this biological process not only for elucidating the mechanism of evolution but also for setting up a conceptual basis to design adequate conservation strategies for endangered populations. In the present study, we assessed genetic and epigenetic alterations in *Xenopus* hybrids; our results suggest that maternally defined H3K4me3 is involved in establishing reproductive isolation and balances the different subgenomes in hybrid embryos of *Xenopus* (Fig. 4H).

Chromosomal rearrangement or chromatin incompatibility is commonly observed in interspecific hybridization, resulting in reproductive isolation. A unique 349-bp repeat enriched with heterochromatin in the X chromosome was identified to induce lethality in the hybridization of female *Drosophila melanogaster* and *Drosophila simulans* (*5*). Paternal and maternal factors perform essential functions during early embryonic development. However, their roles in reproductive isolation are still poorly understood. We believe that incompatibility among the three subgenomes that resulted from the dysregulation of maternally defined H3K4me3, at least in part, caused embryonic lethality in the te×ls hybrids. *X. laevis* is a pseudotetraploid that came into existence via interspecific hybridization of two extinct progenitor diploids (*18*). As a consequence of evolution, the L chromosomes play a role that is dominant to that of the S chromosomes. A large subset of genes located in the S chromosomes were continuously silenced or lost during evolution (*16*, *18*). H3K4me3 modification seems to be essential to the balance of subgenomes in *X. laevis* (*16*–*18*). We believe that H3K4me3 modification also mediates the subgenome balance in hybrid embryos. Similar to *X. laevis*, the le×ts hybrid embryos inherited H3K4me3 modifications from the oocytes of *X. laevis* and could equilibrate the subgenomes from the two species. However, the te×ls embryos could not establish a balance between the L and S chromosomes owing to the lack of H3K4me3 modification. Consequently, the dysregulation of the Wnt signaling pathway, P53 signaling pathway, and other pathways arrest the development of the te×ls embryos (Fig. 4H). In line with this, we observed that the oocytes of *X. laevis* exhibited abundant H3K4me3 modification, whereas the oocytes of *X. tropicalis* exhibited very low levels of H3K4me3 modification, reducing the ability to balance different subgenomes. Because the H3K4me3 is also reported to be critical for zygotic genome activation (ZGA) in gastrulation of *X. tropicalis* (*38*), the lack of H3K4me3 in te×ls hybrids may also induce a failure in ZGA activation, which may also contribute for the development failure.

Corroborating a previous report (*19*), we also found chromosomal deletions with an approximately 75% loss of DNA in ch3L or ch4L in the te×ls hybrid embryos. The loss of large DNA fragments in ch3L and ch4L is an important event for the te×ls hybrids because it leads to significant decreases in corresponding RNA expression. The te×ls hybrids have an additional subgenome compared with normal diploids. Compensation of the homolog genes should be considered while investigating the mechanism underlying embryonic lethality. In fact, almost all of the lost genes were compensated by the homologs. Our study thus provides an additional mechanism to explain the developmental failure of te×ls hybrid embryos.

The mechanism of induction of different DNA deletion patterns in the two hybrids remains obscure. The overall ratios of DNA loss in the two hybrid types were similar. Failure in chromatin separation during cell mitosis may have caused chromosomal deletions in ch3L and ch4L. The centromere protein CENPA in the *X. tropicalis* oocyte is not relocated to the centromeres of the chromosomes of *X. laevis* (*19*), suggesting abnormal spindle formation. A recent study suggested dual spindles rather than a single spindle formed in the first division after fertilization (*39*). The two spindles may have mistakenly assembled in the te×ls embryo because of the similarity of

the homologous chromosomes from three subgenomes, resulting in subsequent chromosomal deletions in ch3L and ch4L during chromosome segregation.

Together, our study emphasizes the importance of maternally defined H3K4me3 modifications in reproductive isolation and in maintaining the subgenome in hybrids. Studying the *Xenopus* hybrids and deciphering the mechanisms underlying speciation will expand our understanding of reproductive isolation as well as DNA repair and epigenetic modifications, which regulate early embryonic development.

MATERIALS AND METHODS

Embryo manipulation

Juvenile *X. laevis* and *X. tropicalis* or adult frogs were purchased from Nasco Co. (USA). The use of *Xenopus* in this study was approved by the ethics committee of The Chinese University of Hong Kong and licensed by the Department of Health, Hong Kong. Embryos were obtained by in vitro fertilization as reported in a previous study (*19*) and staged according to the Nieuwkoop and Faber developmental table (*40*). In brief, both male and female *X. tropicalis* were primed with 20 IU of human chorionic gonadotropin (HCG) the day before use and boosted with 150 IU of HCG the next morning. The female and male *X. laevis* frogs were primed with 500 and 200 IU of HCG, respectively, at night before the experiments. For the generation of WT embryos, the eggs were fertilized with sperm homogenates following the standard procedure (*41*, *42*).

The le×ts hybrid embryos were generated by fertilizing *X. laevis* eggs with *X. tropicalis* testis homogenates that were freshly prepared in 1 ml of double-distilled H_2O (ddH_2O). The mix was incubated for 10 min. The dishes were flooded with one-tenth Marc′s Modified Ringer′s solution (MMR) and incubated for another 20 min before removing the jelly coat using 2% L-cysteine (one-tenth MMR, pH 8.0). The embryos were further cultured in one-tenth MMR at 23°C.

A similar approach was used for generating the te×ls embryos. *X. tropicalis* eggs were collected in a petri dish coated with 1% agar after smoothly massaging the frog′s back. Approximately one-quarter pieces of the dissected *X. laevis* testis solution in L-15 supplemented with 10% fetal bovine serum were added to the eggs, and the eggs were then dispersed in a single layer on the plate. The plate was flooded with 10 ml of ddH_2O 5 min after fertilization and then incubated for 10 min. Another 10 ml of 0.2× MMR was added, and the plate was incubated for 10 min. The jelly coat was removed using 3% L-cysteine (one-tenth MMR, pH 7.8), and the embryos were then cultured in one-tenth MMR at room temperature (approximately 23°C). The KDM5-C70 (MCE, HY-12140) was dissolved in dimethyl sulfoxide with a concentration of 10 mM. It was diluted by one-tenth MMR to the concentrations as indicated for KDM5-C70 treatment.

Microinjection

Microinjection was performed following the procedure reported in our previous study (*43*). The open reading frame of *Xenopus mdm2* was inserted into pCS2+, and the full-length mRNA was generated via in vitro transcription. Approximately 300 ng of *mdm2* mRNA was injected into each hybrid embryo 30 min after fertilization and cultured in 0.2× MMR at 23°C.

Genomic DNA extraction

For WGS, genomic DNA was extracted from embryos as desired using the QIAamp DNA Micro Kit (Qiagen, #160019805). Briefly, the embryos were lysed with proteinase K at 56°C for 8 hours, after which the genomic DNA was extracted following the kit manufacturer′s instructions. The quality of the genomic DNA was analyzed on a 1% agarose gel using capillary electrophoresis, followed by sonication for library construction or PCR analysis.

RNA extraction

Xenopus embryos at the desired stages were collected in a 1.5-ml Eppendorf tube. The embryos were homogenized with TRIzol reagent (Invitrogen, #15596-026) by vortexing and further ruptured with a G25 needle by pulling in and pushing out several times. The aqueous phase containing the RNA was separated using chloroform (Sigma-Aldrich, #C2432) after centrifugation for 10 min at 20,000*g*. The RNA was precipitated using isopropanol and dissolved in 50 μl of RNase-free H_2O after washing with 75% ethanol. The quality of the RNA was analyzed on a 1% agarose gel using capillary electrophoresis prior to library construction.

Library construction and sequencing

For high-throughput sequencing, DNA libraries were constructed using the NEBNext Ultra DNA Library Prep Kit for Illumina (NEB, E7645L), following the manual. RNA libraries for high-throughput sequencing were also constructed using the NEBNext Ultra RNA Library Prep Kit for Illumina (NEB, E7775L). Next-generation sequencing was performed by Novogene (www.novogene.com).

Genomic DNA PCR

Genomic DNA (10 ng) was used as the template for each PCR. A 2× PCR mix (TaKaRa, #RR350) was used, and the DNA amplicon was verified using 1.5% agarose gel electrophoresis. The sequences of the primers used in this assay are listed in tables S2 and S3.

Quantitative PCR

Total RNA was extracted from whole embryos using TRIzol reagent (Invitrogen, #15596-026). Complementary DNA (cDNA) was generated using a PrimeScript RT reagent kit (TaKaRa, #RR037A). PCR was performed using the reverse-transcribed cDNA as a template on either a standard PCR machine (animal cap assay) or the ABI 7900HT Fast Real-Time PCR system. The primers used in this experiment are listed in table S3.

Whole-mount in situ hybridization

Embryos at desired stages were fixed using HEMFA reagent [0.1 M Hepes (pH 7.4), 2 mM EGTA, 1 mM $MgSO_4$, and 4% formaldehyde] for 1 hour at room temperature. Whole-mount in situ hybridization was performed as described previously (*41*, *44*).

Western blot

The embryos were lysed with radioimmunoprecipitation assay buffer [10 mM tris (pH 7.6), 150 mM NaCl, 5 mM EDTA, 0.5% Triton X-100, and 0.5% SDS] using a pipette and vortexed roughly after adding 100 μl of 1,1,2-trichlorotrifluoroethane. After centrifugation for 10 min at 20,000*g*/min, the supernatant was collected, and the protein concentration was quantified using a bicinchoninic acid (BCA) assay kit (Thermo Fisher Scientific, 23223).

Equal amounts of the protein extracts were subjected to SDS–polyacrylamide gel electrophoresis, and Western blotting was performed using a method published previously (*42*). Primary antibodies targeting histone H3 (Sigma-Aldrich, SAB4200591), H3K4me3 (Abcam, ab8580), H3K9ac (Abcam, ab10812), H3K27ac (Abcam, ab4729), Mdm2 (CST, #86934), P53 (Santa Cruz, SC126), and Actin (HuaBio, ET1702-67) were used. All of the antibodies used have been listed in table S4.

Immunofluorescence

Embryos were fixed with 1× MEMFA [0.1 M Mops (pH 7.4), 2 mM EGTA, 1 mM $MgSO_4$, and 3.7% formaldehyde] for 2 hours at room temperature and washed three times with phosphate buffered saline with 0.1% Tween-20 (PBST). The pigment was bleached by 10% H_2O_2 after dehydration with 100% methanol. The embryos were rehydrated with gradient methanol and then treated with 0.1% $NaBH_4$ to prevent autofluorescence. After blocking with 10% fetal bovine serum for 1 hour, the embryos were incubated with H3K4me3 antibody (1;100, Abcam, ab8580) overnight at 4°C. The embryos were washed with PBST and incubated with the secondary antibody for 2 hours. The embryo clearance was carried out by Murry buffer (1:1 benzyl alcohol:benzyl benzoate), and fluorescence images were captured with a confocal microscope (Leica SP8, Germany). The fluorescence intensity of H3K4me3 in the nucleus was counted by ImageJ with the particle analysis plugin (*45*).

RNA-seq analysis

RNA-seq raw data were processed using the standard RNA-seq analysis pipeline. In brief, the reads were mapped to *X. laevis* (Xenbase v9.2) and *X. tropicalis* (Xenbase v9.1). The alignments were examined using TopHat2 version 2.1.0 (*46*), and all reads mapped to multiple targets were discarded. The reads mapped to each gene were annotated using Htseq count. Differential expression analyses were conducted on the basis of the DESeq2 R library. Differential expression tests and visualization were then performed using the START web-based RNA-seq analysis resources (*47*). KEGG enrichment analysis was performed using The Database for Annotation, Visualization and Integrated Discovery (DAVID) v6.8 (*48*, *49*). GSEA was performed using GSEA software (*50*). The mean expression level (TPM; transcript per million) per transcript was obtained by combining all replicates. Heatmaps and clustering plots were generated using ggplot2 with custom scripts.

Genomic sequencing analysis

Genome alignment of the hybrids with *X. tropicalis* and *X. laevis* was performed using the Burrow-Wheeler aligner with the default parameters. The L and S subgenomes of *X. tropicalis* and *X. laevis* were treated as separate genomes and aligned using a Newick format phylogenetic tree. Indels were called using the GATK pipeline, according to the best practice workflow. The HaplotypeCaller tool was used to call indels. All putative indels were subsequently filtered using the variant filtration tool. The filter expression was set to "QD <2 || FS > 60.0 || MQ < 35.0 || MQRankSum < -12.5 ||ReadPosRankSum < −8.0". Indels passing the filter were required to have at least 10× coverage, with at least four observations of the alternative allele. The indel coverage was calculated relative to the sequence regions in which indels could be called given the minimum required coverage, as determined using GATK's Callable Loci tool.

ChIP-seq and data analysis

For each sample, approximately 30 embryos at stage 9 were collected and dissociated into single cells after pipetting with calcium- and magnesium-free medium [7.5 mM tris (pH 7.6), 2.4 mM $NaHCO_3$, 88 mM NaCl, and 1 mM KCl]. The cells were collected by centrifugation. The ChIP library was constructed following the manual of the Hyperactive In-situ ChIP Library Prep Kit for Illumina (Vazyme, #TD901), and 10 μg of H3K4me3 antibody (Abcam, ab8580) was added to each sample. High-throughput sequencing was performed using the NovaSeq platform and the PE 150 sequencing strategy. Quality control of the ChIP-seq data was performed using FastQC, after which low-quality bases and adaptor contamination were filtered using Trim galore. After quality control and data filtering were performed, the data were mapped to the *X. laevis* genome using bowtie2 software. Peak calling was performed using MACS 2.0, and significant enrichments were identified with a threshold level set at a q value of <0.05. Peak annotation was performed as reported (*51*). Some of the ChIP-seq data of *X. laevis* and *X. tropicalis* used in our analysis were downloaded from the Gene Expression Omnibus database under the accession numbers SRR5110212–SRR5110215 and SRR5110218–SRR5110221.

Weighted correlation network analysis

To compare the DEGs and investigate the interactions among the genes in different species (te×ls vs. *X. tropicalis*), we used the weighted correlation network analysis (WGCNA) to identify different modules. The WGCNA R package was used, and the power parameter was precalculated using the pickSoftThreshold function. This function can provide the appropriate soft-thresholding power for network construction by calculating the scale-free topology fit index for several powers. Last, 10 was used as the soft power. Adjacency was turned into topological overlap to measure the network connectivity of a gene, defined as the sum of its adjacency with all other genes for network generation. The hierarchical clustering function was used to classify genes with similar expression profiles into modules based on topological overlap matrix dissimilarity, with a minimum size of 50 for the gene dendrogram. The dissimilarity of the module eigengenes was calculated to choose a cutoff for merging some modules. The gene expression heatmap was visualized using all genes in this module. The last visualization in the gene network of the eigengenes was also conducted using the clusterProfiler package in R.

Statistical analysis

Data are presented as means ± SD or means ± SEM. Sample number (n) indicates independent biological samples used in each experiment. All experiments have been performed at least three times, except those indicated in the figure legend. Two-tailed unpaired Student's t test or one-way analysis of variance (ANOVA) test are used in statistical analysis with GraphPad Prism 8. Wilcoxon rank sum test and hyper geometric test are used with statistical software R (*$P \leq 0.05$, **$P \leq 0.01$, and ***$P \leq 0.001$).

Supplementary Materials

This PDF file includes:

Figs. S1 to S8
Tables S1 to S5
Legend for table S6

Other Supplementary Material for this manuscript includes the following:
Table S6

View/request a protocol for this paper from *Bio-protocol*.

REFERENCES AND NOTES

1. A. A. Barnard, O. M. Fincke, M. A. McPeek, J. P. Masly, Mechanical and tactile incompatibilities cause reproductive isolation between two young damselfly species. *Evolution* **71**, 2410–2427 (2017).
2. J. D. Brown, R. J. O'Neill, Chromosomes, conflict, and epigenetics: Chromosomal speciation revisited. *Annu. Rev. Genomics Hum. Genet.* **11**, 291–316 (2010).
3. T. Dobzhansky, Studies on hybrid sterility. II. Localization of sterility factors in Drosophila pseudoobscura hybrids. *Genetics* **21**, 113–135 (1936).
4. C. Sakai, F. Konno, O. Nakano, T. Iwai, T. Yokota, J. Lee, C. Nishida-Umehara, A. Kuroiwa, Y. Matsuda, M. Yamashita, Chromosome elimination in the interspecific hybrid medaka between Oryzias latipes and O-hubbsi. *Chromosome Res.* **15**, 697–709 (2007).
5. P. M. Ferree, D. A. Barbash, Species-specific heterochromatin prevents mitotic chromosome segregation to cause hybrid lethality in Drosophila. *PLOS Biol.* **7**, e1000234 (2009).
6. S. Maheshwari, D. A. Barbash, The genetics of hybrid incompatibilities. *Annu. Rev. Genet.* **45**, 331–355 (2011).
7. J. L. Feder, P. Nosil, Chromosomal inversions and species differences: When are genes affecting adaptive divergence and reproductive isolation expected to reside within inversions? *Evolution* **63**, 3061–3075 (2009).
8. M. A. Noor, K. L. Grams, L. A. Bertucci, J. Reiland, Chromosomal inversions and the reproductive isolation of species. *Proc. Natl. Acad. Sci. U.S.A.* **98**, 12084–12088 (2001).
9. S. E. Hughes, R. S. Hawley, Heterochromatin: A rapidly evolving species barrier. *PLOS Biol.* **7**, e1000233 (2009).
10. C. Canestro, R. Albalat, M. Irimia, J. Garcia-Fernandez, Impact of gene gains, losses and duplication modes on the origin and diversification of vertebrates. *Semin. Cell Dev. Biol.* **24**, 83–94 (2013).
11. Y. Han, Z. Zhang, C. Liu, J. Liu, S. Huang, J. Jiang, W. Jin, Centromere repositioning in cucurbit species: Implication of the genomic impact from centromere activation and inactivation. *Proc. Natl. Acad. Sci. U.S.A.* **106**, 14937–14941 (2009).
12. M. Lu, X. He, Centromere repositioning causes inversion of meiosis and generates a reproductive barrier. *Proc. Natl. Acad. Sci. U.S.A.* **116**, 21580–21591 (2019).
13. A. Villasante, J. P. Abad, M. Mendez-Lago, Centromeres were derived from telomeres during the evolution of the eukaryotic chromosome. *Proc. Natl. Acad. Sci. U.S.A.* **104**, 10542–10547 (2007).
14. C. Josefsson, B. Dilkes, L. Comai, Parent-dependent loss of gene silencing during interspecies hybridization. *Curr. Biol.* **16**, 1322–1328 (2006).
15. P. Narbonne, D. E. Simpson, J. B. Gurdon, Deficient induction response in a Xenopus nucleocytoplasmic hybrid. *PLOS Biol.* **9**, e1001197 (2011).
16. D. M. Elurbe, S. S. Paranjpe, G. Georgiou, I. van Kruijsbergen, O. Bogdanovic, R. Gibeaux, R. Heald, R. Lister, M. A. Huynen, S. J. van Heeringen, G. J. C. Veenstra, Regulatory remodeling in the allo-tetraploid frog Xenopus laevis. *Genome Biol.* **18**, 198 (2017).
17. R. D. Morin, E. Chang, A. Petrescu, N. Liao, M. Griffith, W. Chow, R. Kirkpatrick, Y. S. Butterfield, A. C. Young, J. Stott, S. Barber, R. Babakaiff, M. C. Dickson, C. Matsuo, D. Wong, G. S. Yang, D. E. Smailus, K. D. Wetherby, P. N. Kwong, J. Grimwood, C. P. Brinkley III, M. Brown-John, N. D. Reddix-Dugue, M. Mayo, J. Schmutz, J. Beland, M. Park, S. Gibson, T. Olson, G. G. Bouffard, M. Tsai, R. Featherstone, S. Chand, A. S. Siddiqui, W. Jang, E. Lee, S. L. Klein, R. W. Blakesley, B. R. Zeeberg, S. Narasimhan, J. N. Weinstein, C. P. Pennacchio, R. M. Myers, E. D. Green, L. Wagner, D. S. Gerhard, M. A. Marra, S. J. Jones, R. A. Holt, Sequencing and analysis of 10,967 full-length cDNA clones from Xenopus laevis and Xenopus tropicalis reveals post-tetraploidization transcriptome remodeling. *Genome Res.* **16**, 796–803 (2006).
18. A. M. Session, Y. Uno, T. Kwon, J. A. Chapman, A. Toyoda, S. Takahashi, A. Fukui, A. Hikosaka, A. Suzuki, M. Kondo, S. J. van Heeringen, I. Quigley, S. Heinz, H. Ogino, H. Ochi, U. Hellsten, J. B. Lyons, O. Simakov, N. Putnam, J. Stites, Y. Kuroki, T. Tanaka, T. Michiue, M. Watanabe, O. Bogdanovic, R. Lister, G. Georgiou, S. S. Paranjpe, I. van Kruijsbergen, S. Shu, J. Carlson, T. Kinoshita, Y. Ohta, S. Mawaribuchi, J. Jenkins, J. Grimwood, J. Schmutz, T. Mitros, S. V. Mozaffari, Y. Suzuki, Y. Haramoto, T. S. Yamamoto, C. Takagi, R. Heald, K. Miller, C. Haudenschild, J. Kitzman, T. Nakayama, Y. Izutsu, J. Robert, J. Fortriede, K. Burns, V. Lotay, K. Karimi, Y. Yasuoka, D. S. Dichmann, M. F. Flajnik, D. W. Houston, J. Shendure, L. DuPasquier, P. D. Vize, A. M. Zorn, M. Ito, E. M. Marcotte, J. B. Wallingford, Y. Ito, M. Asashima, N. Ueno, Y. Matsuda, G. J. C. Veenstra, A. Fujiyama, R. M. Harland, M. Taira, D. S. Rokhsar, Genome evolution in the allotetraploid frog Xenopus laevis. *Nature* **538**, 336–343 (2016).
19. R. Gibeaux, R. Acker, M. Kitaoka, G. Georgiou, I. van Kruijsbergen, B. Ford, E. M. Marcotte, D. K. Nomura, T. Kwon, G. J. C. Veenstra, R. Heald, Paternal chromosome loss and metabolic crisis contribute to hybrid inviability in Xenopus. *Nature* **553**, 337–341 (2018).
20. S. Marsit, A. M. Dion-Cote, D. A. Barbash, Did mitochondria kill the frog? *Dev. Cell* **44**, 539–541 (2018).
21. J. A. White, J. Heasman, Maternal control of pattern formation in Xenopus laevis. *J. Exp. Zool. B Mol. Dev. Evol.* **310**, 73–84 (2008).
22. G. E. Gentsch, T. Spruce, N. D. L. Owens, J. C. Smith, Maternal pluripotency factors initiate extensive chromatin remodelling to predefine first response to inductive signals. *Nat. Commun.* **10**, 4269 (2019).
23. B. T. MacDonald, K. Tamai, X. He, Wnt/beta-catenin signaling: Components, mechanisms, and diseases. *Dev. Cell* **17**, 9–26 (2009).
24. D. Zheng, K. F. Decker, T. Zhou, J. Chen, Z. Qi, K. Jacobs, K. N. Weilbaecher, E. Corey, F. Long, L. Jia, Role of WNT7B-induced noncanonical pathway in advanced prostate cancer. *Mol. Cancer Res.* **11**, 482–493 (2013).
25. J. Chang, W. Sonoyama, Z. Wang, Q. Jin, C. Zhang, P. H. Krebsbach, W. Giannobile, S. Shi, C. Y. Wang, Noncanonical Wnt-4 signaling enhances bone regeneration of mesenchymal stem cells in craniofacial defects through activation of p38 MAPK. *J. Biol. Chem.* **282**, 30938–30948 (2007).
26. K. Zhang, Y. Harada, X. Wei, D. Shukla, A. Rajendran, K. Tawansy, M. Bedell, S. Lim, P. X. Shaw, X. He, Z. Yang, An essential role of the cysteine-rich domain of FZD4 in Norrin/Wnt signaling and familial exudative vitreoretinopathy. *J. Biol. Chem.* **286**, 10210–10215 (2011).
27. V. S. W. Li, S. S. Ng, P. J. Boersema, T. Y. Low, W. R. Karthaus, J. P. Gerlach, S. Mohammed, A. J. R. Heck, M. M. Maurice, T. Mahmoudi, H. Clevers, Wnt signaling through inhibition of β-Catenin degradation in an intact Axin1 complex. *Cell* **149**, 1245–1256 (2012).
28. H. Karvonen, R. Perttilä, W. Niininen, V. Hautanen, H. Barker, A. Murumägi, C. A. Heckman, D. Ungureanu, Wnt5a and ROR1 activate non-canonical Wnt signaling via RhoA in TCF3-PBX1 acute lymphoblastic leukemia and highlight new treatment strategies via Bcl-2 co-targeting. *Oncogene* **38**, 3288–3300 (2019).
29. S. Mazzotta, C. Neves, R. J. Bonner, A. S. Bernardo, K. Docherty, S. Hoppler, Distinctive roles of canonical and noncanonical Wnt signaling in human embryonic cardiomyocyte development. *Stem Cell Rep.* **7**, 764–776 (2016).
30. M. Molenaar, M. van de Wetering, M. Oosterwegel, J. Peterson-Maduro, S. Godsave, V. Korinek, J. Roose, O. Destrée, H. Clevers, XTcf-3 transcription factor mediates beta-catenin-induced axis formation in Xenopus embryos. *Cell* **86**, 391–399 (1996).
31. A. Hafner, M. L. Bulyk, A. Jambhekar, G. Lahav, The multiple mechanisms that regulate p53 activity and cell fate. *Nat. Rev. Mol. Cell Biol.* **20**, 199–210 (2019).
32. L. D. Attardi, A. de Vries, T. Jacks, Activation of the p53-dependent G1 checkpoint response in mouse embryo fibroblasts depends on the specific DNA damage inducer. *Oncogene* **23**, 973–980 (2004).
33. H. Clevers, Wnt/β-Catenin signaling in development and disease. *Cell* **127**, 469–480 (2006).
34. B. L. Martin, D. Kimelman, Wnt signaling and the evolution of embryonic posterior development. *Curr. Biol.* **19**, R215–R219 (2009).
35. T. Nagase, M. Nagase, M. Machida, M. Yamagishi, Hedgehog signaling: A biophysical or biomechanical modulator in embryonic development? *Ann. N. Y. Acad. Sci.* **1101**, 412–438 (2007).
36. A. B. Williams, B. Schumacher, p53 in the DNA-damage-repair process. *Cold Spring Harb. Perspect. Med.* **6**, a026070 (2016).
37. J. A. Dahl, I. Jung, H. Aanes, G. D. Greggains, A. Manaf, M. Lerdrup, G. Li, S. Kuan, B. Li, A. Y. Lee, S. Preissl, I. Jermstad, M. H. Haugen, R. Suganthan, M. Bjørås, K. Hansen, K. T. Dalen, P. Fedorcsak, B. Ren, A. Klungland, Broad histone H3K4me3 domains in mouse oocytes modulate maternal-to-zygotic transition. *Nature* **537**, 548–552 (2016).
38. R. C. Akkers, S. J. van Heeringen, U. G. Jacobi, E. M. Janssen-Megens, K. J. Françoijs, H. G. Stunnenberg, G. J. C. Veenstra, A hierarchy of H3K4me3 and H3K27me3 acquisition in spatial gene regulation in Xenopus embryos. *Dev. Cell* **17**, 425–434 (2009).
39. J. Reichmann, B. Nijmeijer, M. J. Hossain, M. Eguren, I. Schneider, A. Z. Politi, M. J. Roberti, L. Hufnagel, T. Hiiragi, J. Ellenberg, Dual-spindle formation in zygotes keeps parental genomes apart in early mammalian embryos. *Science* **361**, 189–193 (2018).
40. P. D. Nieuwkoop, and J. Faber, *Normal Table of Xenopus laevis (Daudin): A Systematical and Chronological Survey of the Development from the Fertilized Egg Till the end of Metamorphosis* (Garland Science, 1994).
41. C. Wang, X. Qi, X. Zhou, J. Sun, D. Cai, G. Lu, X. Chen, Z. Jiang, Y.-G. Yao, W. Y. Chan, H. Zhao, RNA-Seq analysis on ets1 mutant embryos of *Xenopus tropicalis* identifies *microseminoprotein beta gene 3* as an essential regulator of neural crest migration. *FASEB J.* **34**, 12726–12738 (2020).
42. C. Wang, R. K. T. Kam, W. Shi, Y. Xia, X. Chen, Y. Cao, J. Sun, Y. du, G. Lu, Z. Chen, W. Y. Chan, S. O. Chan, Y. Deng, H. Zhao, The proto-oncogene transcription factor Ets1 regulates neural

crest development through histone deacetylase 1 to mediate output of bone morphogenetic protein signaling. *J. Biol. Chem.* **290**, 21925–21938 (2015).
43. H. Wang, C. Wang, Q. Long, Y. Zhang, M. Wang, J. Liu, X. Qi, D. Cai, G. Lu, J. Sun, Y.-G. Yao, W. Y. Chan, W. Y. Chan, Y. Deng, H. Zhao, Kindlin2 regulates neural crest specification via integrin-independent regulation of the FGF signaling pathway. *Development* **148**, dev199441 (2021).
44. C. D. Wang, X.-F. Guo, T. C. B. Wong, H. Wang, X.-F. Qi, D.-Q. Cai, Y. Deng, H. Zhao, Developmental expression of three *prmt* genes in Xenopus. *Zool. Res.* **40**, 102–107 (2019).
45. C. T. Rueden, J. Schindelin, M. C. Hiner, B. E. DeZonia, A. E. Walter, E. T. Arena, K. W. Eliceiri, ImageJ2: ImageJ for the next generation of scientific image data. *BMC Bioinformatics* **18**, 529 (2017).
46. C. Trapnell, L. Pachter, S. L. Salzberg, TopHat: Discovering splice junctions with RNA-Seq. *Bioinformatics* **25**, 1105–1111 (2009).
47. A. Dobin, C. A. Davis, F. Schlesinger, J. Drenkow, C. Zaleski, S. Jha, P. Batut, M. Chaisson, T. R. Gingeras, STAR: Ultrafast universal RNA-seq aligner. *Bioinformatics* **29**, 15–21 (2013).
48. D. W. Huang, B. T. Sherman, R. A. Lempicki, Systematic and integrative analysis of large gene lists using DAVID bioinformatics resources. *Nat. Protoc.* **4**, 44–57 (2009).
49. D. W. Huang, B. T. Sherman, R. A. Lempicki, Bioinformatics enrichment tools: paths toward the comprehensive functional analysis of large gene lists. *Nucleic Acids Res.* **37**, 1–13 (2009).
50. A. Subramanian, P. Tamayo, V. K. Mootha, S. Mukherjee, B. L. Ebert, M. A. Gillette, A. Paulovich, S. L. Pomeroy, T. R. Golub, E. S. Lander, J. P. Mesirov, Gene set enrichment analysis: A knowledge-based approach for interpreting genome-wide expression profiles. *Proc. Natl. Acad. Sci. U.S.A.* **102**, 15545–15550 (2005).
51. S. Heinz, C. Benner, N. Spann, E. Bertolino, Y. C. Lin, P. Laslo, J. X. Cheng, C. Murre, H. Singh, C. K. Glass, Simple combinations of lineage-determining transcription factors prime cis-regulatory elements required for macrophage and B cell identities. *Mol. Cell* **38**, 576–589 (2010).

Acknowledgments: We are grateful to all members of H. Zhao's and X. Lu's laboratories for the valuable discussions. We also thank the staff of the core laboratory at the School of Biomedical Sciences, The Chinese University of Hong Kong. **Funding:** This work was supported by the National Key R&D Program of China, Synthetic Biology Research (2019YFA0904500 to H.Z.); the National Natural Science Foundation of China (U1902201 to X.Lu); The Second Tibetan Plateau Scientific Expedition and Research (STEP) program (2019QZKK0501 to X.Lu); Research Grants Council of Hong Kong (14167017, 14112618, and 14119120 to H.Z.); The Hong Kong Branch of the CAS Center for Excellence in Animal Evolution and Genetics, The Chinese University of Hong Kong (8601012 to H.Z.); the Guangdong Province Science and Technology Program (grant/award number: 2023A1515030231 to Q.L.); and the Open Research Program of Key Laboratory of Regenerative Biology, CAS (grant/award number: KLRB202203 to Q.L.). **Author contributions:** H.Z. and X.Lu designed and supervised the project. Q.L. and K.Y. designed and carried out the experiments and did the data analysis. H.Z., X.Lu, Q.L., and K.Y. wrote the manuscript. C.W. performed part of the qPCR and WISH. C.W., Y.W., F.Q., H.W., P.S., X.Liu, and W.-Y.C. participated in the manuscript revision. **Competing interests:** The authors declare that they have no competing interests. **Data and materials availability:** All sequencing data have been submitted to the National Genomics Data Center and obtained the accession number CRA006640. All data needed to evaluate the conclusions in the paper are present in the paper and/or the Supplementary Materials. The construct of mdm2 can be provided by H.Z. pending scientific review and a completed material transfer agreement. Requests for the construct should be submitted to H.Z.

Submitted 7 July 2022
Accepted 6 March 2023
Published 7 April 2023
10.1126/sciadv.add8343